Available online at www.sciencedirect.com
SciVerse ScienceDirect
Procedia Engineering 58 (2013) 702 – 708
Procedia Engineering
www.elsevier.com/locate/procedia

The 12th Hypervelocity Impact Symposium

# Damage Evolution in $SiO_2$ Glass Subjected to Hypervelocity Impact

Nobuaki Kawai[a]*, Kenji Tsurui[a], Kairi Moriguchi[a], Sunao Hasegawa[a], Eiichi Sato[a]

[a]*Institute of Space and Astronautical Science, Japan Aerospace Exploration Agency, 3-1-1 Yoshinodai, Chuo, Sagamihara, Kanagawa 252-5210, Japan*

**Abstract**

Hypervelocity-impact experiments are performed on $SiO_2$ glass plates to investigate its damage process. The damage propagation behavior induced by a hypervelocity impact is observed using a high-speed video camera. The postmortem observations reveal that the damage structure of the impacted plates consists mainly of crater, internal failure zone, and radial cracks. The sequence of the damage formation and propagation during a hypervelocity-impact event is revealed using the images of the high-speed video camera. The propagation velocities of surface fracture show a nearly constant value regardless of impacting conditions. The propagation velocities of internal failure zone increase with decreasing target thickness. The formation of radial cracks is affected by the projectile kinetic energy normalized by the target thickness. The radial crack velocities increase with increasing the normalized kinetic energy and approach asymptotically to the terminal velocity.



Selection and peer-review under responsibility of the Hypervelocity Impact Society

*Keywords*: Hypervelocity impact; $SiO_2$ glass; Damage evolution; High-speed imaging, Propagation velocity

**Nomenclature**

| | |
|---|---|
| $\rho_p$ | projectile density |
| $t_t$ | target thickness |
| $v_p$ | projectile velocity |
| $KE_p$ | kinetic energy of projectile |
| $C_l$ | longitudinal sound velocity of target material |
| $C_t$ | transversal sound velocity of target material |
| $v_D$ | initial damage velocity |

## 1. Introduction

Against a backdrop of increasing number of space debris, damage caused by hypervelocity impacts of micrometeoroids and space debris is a growing concern in spacecraft design. While about 16,000 pieces of space debris in Earth orbit over 10 cm in diameter are tracked routinely by the U.S. Space Surveillance Network, it is estimated that there are over 500,000 pieces of un-cataloged space debris between the size of 1 and 10 cm in diameter [1]. Moreover, the number of orbital debris smaller than 1 cm exceeds 100 million. Although the size of the debris and micrometeoroids is relatively small, they are traveling at hypervelocity in space and these impacts can compromise the structural integrity as well as the optical, thermal and electrical functionality of a spacecraft.

Hypervelocity-impact damage of metals has been extensively investigated [2, 3]. While metals are large components of spacecraft, brittle materials such as glass and ceramics are often significant components of optical and thermal protection

* Corresponding author. Tel.: +81-50-3362-2399 ; fax: +81-42-759-8461.
*E-mail address:* nkawai@isas.jaxa.jp.


Selection and peer-review under responsibility of the Hypervelocity Impact Society
doi:10.1016/j.proeng.2013.05.081

systems of space structures. These brittle materials are much more sensitive to hypervelocity impact than metals. Although several studies have been done to investigate hypervelocity-impact damage of brittle materials, these studies mainly focus on generating equations to predict impact crater geometry [4-6]. The aim of this study is the investigation of damage evolution in brittle materials subjected to hypervelocity impacts.

In this study, hypervelocity-impact experiments were performed on $SiO_2$ glass to investigate the impact-induced damage evolution of brittle material. $SiO_2$ glass is not only a typical brittle material but also the primal optical material of space-structures. The damage propagation behavior was visualized using a high-speed video camera. Because of transparency of glass target, it is expected to observe the propagation behavior of internal failure and surface fracture simultaneously. These results can provide an insight into the damage evolution of the brittle material subjected to hypervelocity impact.

## 2. Experimental

The $SiO_2$ glass used in this study was manufactured by Mitorika Glass Co., Ltd. The sizes of target were 80 mm square plates with three different thicknesses: 5, 10 and 15 mm. These plates were supplied in a polished condition requiring no further preparation. A grid pattern of 10-mm wide was drawn on the impacted surface for post analysis of the observed high-speed video images.

Hypervelocity-impact experiments were conducted using a two-stage light-gas gun. A spherical projectile of 0.5-mm diameter was shot at the target plate at velocities ranging from 4.5 to 7 km/s using a single microparticle lunching technique [7]. The projectile materials were aluminum ($\rho_p$ = 2.78 Mg/m$^3$), stainless steel ($\rho_p$ = 7.89 Mg/m$^3$), and platinum ($\rho_p$ = 21.1 Mg/m$^3$). The target plate was fixed in an acrylic frame with an adhesive tape so that there was a free rear surface and the target was fixed in a practically unconfined manner. All the impact-test conditions are listed in Table1.

A schematic of the experimental setup is given in Fig. 1. The impact event and ensuing damage evolution was recorded at 1 million frames per second using a high-speed camera (Shimadzu Corp., HPV-1). The shooting angle of the high-speed video camera was set at 45 degree with respect to the ballistic direction. The damage evolutional behavior was observed in a reflected light configuration. In this configuration, the high-speed camera can detect the light reflected from front surface which transfer the information of surface condition and the light reflected from rear surface which pass through the target and reflect the internal condition. Consequently, it is possible to observe distinctly the behavior of surface and internal damage. In order to evaluate the in-plane damage evolution, the radial distances of the damage front and/or crack tips from the impact point were measured at the each high-speed video image. The length scale of the obtained high-speed video image was calibrated using the grid image drawn on the sample surface. The tilt of the video image resulting from the 45º imaging was corrected with the aspect ratio of the grid image.

Table 1. Experimental conditions of hypervelocity-impact tests

| Shot No. | $t_t$ / mm | Projectile material | $v_p$ / km/s | $KE_p$ / J |
|---|---|---|---|---|
| 1228 | 5 | Al | 5.81 | 3.07 |
| 1229 | | | 6.88 | 4.30 |
| 1241 | | Steel | 5.08 | 6.66 |
| 1235 | | | 5.60 | 8.10 |
| 1231 | | | 6.86 | 12.2 |
| 1617 | | Pt | 5.76 | 23.2 |
| 1368 | 10 | Steel | 6.85 | 12.1 |
| 1501 | | Pt | 4.82 | 16.3 |
| 1373 | | | 5.19 | 18.9 |
| 1616 | | | 6.65 | 30.9 |
| 1370 | | | 6.84 | 32.8 |
| 1164 | 15 | Al | 5.64 | 2.89 |
| 1165 | | | 5.85 | 3.11 |
| 1163 | | | 5.98 | 3.26 |
| 1166 | | | 6.05 | 3.33 |
| 1234 | | Steel | 6.82 | 12.0 |
| 1372 | | Pt | 4.67 | 15.2 |
| 1618 | | | 5.84 | 23.9 |
| 1371 | | | 6.93 | 33.7 |

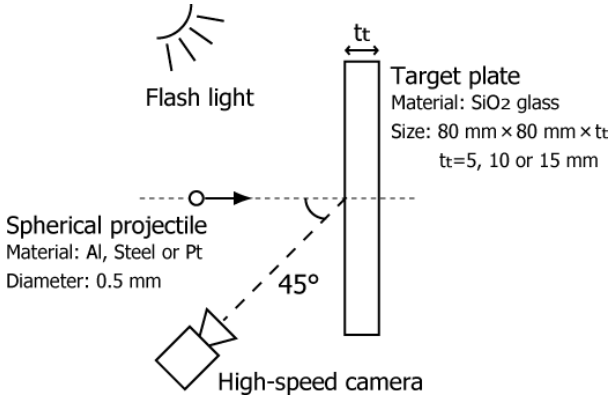


Fig. 1. Schematic of experimental configuration.

## 3. Results and Discussion

### *3.1. Impact failure morphology of $SiO_2$ glass*

Hypervelocity-impact damage in $SiO_2$ glass results in a front-side crater with large diameter relative to crater depth, and internal fracture. Figure 2 shows photos of the various types of damage features obtained in the impact tests. The experimental conditions of each result are as follows: (a) $t_t$ = 15 mm, $v_p$ = 6.8 km/s, stainless-steel projectile, (b) $t_t$ = 5 mm, $v_p$ = 6.9 km/s, stainless-steel projectile, (c) $t_t$ = 10 mm, $v_p$ = 6.8 km/s, platinum projectile. In the case of thick target or low projectile kinetic energy (Fig. 2(a)), an impact pit has a central area of high damage, surrounded by circular surface fracture patterns named as conchoidal failure [8].

In the case of thin target (Fig. 2(b)), numerous conical cracks propagated inside the target from the damaged central area. In addition, circular internal cracks were formed, which appear to nucleate within the microfracture zone created by the impact. The radius of this internal fracture zone is considerably larger than that of crater. The propagation of radial cracks from the highly damaged region around the crater was also observed.

Under higher kinetic energy impact (Fig. 2(c)), the formation of lateral cracks was observed. These cracks were oriented along a circumferential locus and located outside of the crater area.

As the results of postmortem observations, damage patterns associated with hypervelocity impact events are categorized into six types; central pit, conchoidal failure, cone crack, circular internal fracture, circumferential lateral crack and radial crack. These damage features are shown schematically in Fig. 3. Because of the high ratio of target thickness to projectile diameter, rear surface spallation was not observed in this study.

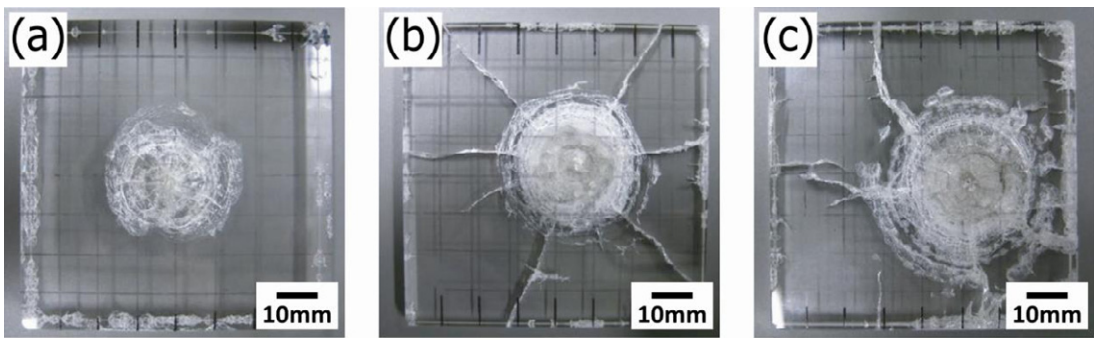


Fig. 2. Damage structure of $SiO_2$ glass subjected hypervelocity impact.

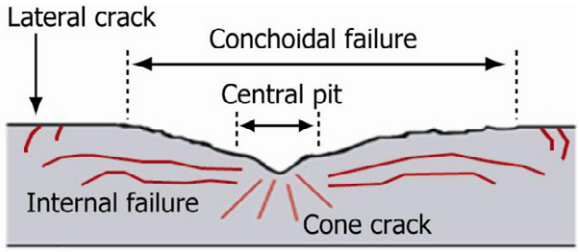


Fig. 3. Schematic of hypervelocity impact damage in $SiO_2$ glass.

### *3.2. High speed imaging of impact damage evolution*

Figure 4 shows a 15-mm-thick $SiO_2$ glass plate impacted by a stainless-steel projectile at 6.8 km/s. The postmortem damage structure of this plate corresponds to Fig. 2(a). Immediately upon impact, a shock wave isotropically propagates from impacting point. After that, radial cracks propagate followed by the development of surface-fractured area. Associated with the radial cracks growing, a circular crack form at the tips of the radial cracks and propagates as a conchoidal crack. Finally, the area where the conchoidal crack propagates is spalled.

Figure 5 shows a 5-mm-thick $SiO_2$ glass plate impacted by a stainless-steel projectile at 6.9 km/s. The damage structure after impact corresponds to Fig. 2(b). Following the propagation of a spherical shock wave from the impact point, the rapid growing of internal failure zone and the slower propagation of surface-fractured area are observed. After the formation of the internal failure zone, radial cracks grow beyond that damaged area.

Figure 6 shows a 10-mm-thick $SiO_2$ glass plate impacted by a platinum projectile at 6.8 km/s. This test corresponds to Fig. 2(c). Although the postmortem damage structure of this test is similar to the results of Fig. 2(b), the damage evolution is quite different. The internal failure zone shows continuous growth in Fig. 5. In contrast, Fig. 6 shows that the spreading of the internal failure zone results from the linking and growing of discretely-formed cracks. In addition, a ring-shaped lateral crack is formed outside the internal failure zone. This type of damage evolution tends to be observed in the impact-tests using a platinum projectile, indicating that the formation of lateral cracks needs relatively high impact energy.

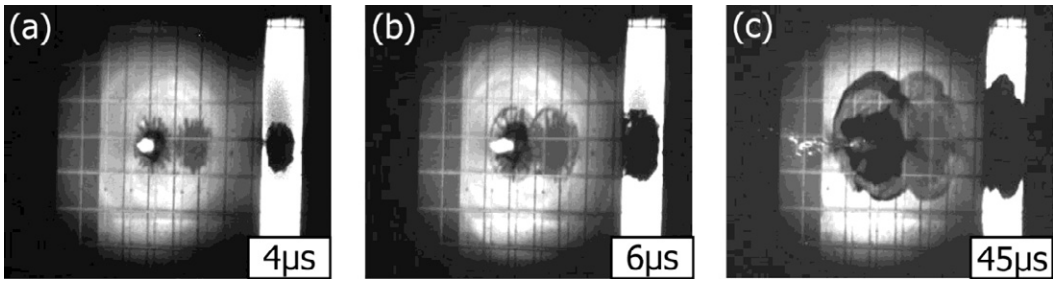


Fig. 4. Damage evolution in 15-mm-thick glass target impacted by a stainless-steel projectile at 6.8 km/s.

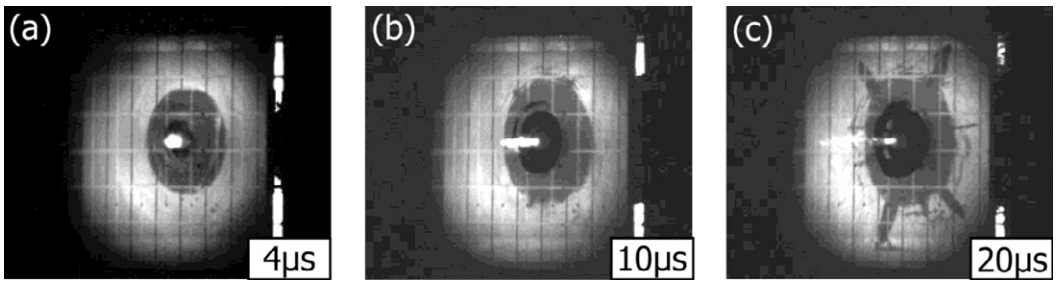


Fig. 5. Damage evolution in 5-mm-thick glass target impacted by a stainless-steel projectile at 6.9 km/s.

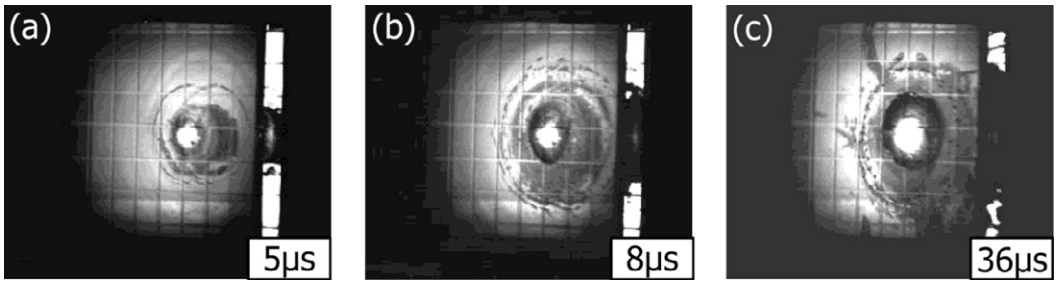


Fig. 6. Damage evolution in 10-mm-thick glass target impacted by a platinum projectile at 6.8 km/s.

### *3.3. Damage propagation behavior*

The path-time histories of the damage propagation into radial direction are derived from the observed high-speed video images. Figure 7 shows the path-time histories of the surface fracture and internal failure in 5-, 10- and 15-mm-thick $SiO_2$ glass plates. The propagation distance increases with increasing the kinetic energy of projectile. Especially, the propagation distance of thick plate is more sensitive to the projectile energy than that of thin plate. In all cases, the propagation behavior shows similar tendency that is rapid propagation followed by slow one. The transition of propagation rate occur around 10 μs after impact. This transition becomes more drastic with decreasing target thickness.

The initial rapid propagation accounts for the large portion of the total damage propagation distance. The average velocities in initial rapid propagation part for surface fracture, conchoidal failure and internal failure are derived by linear regression of the path-time data from 0 to 6 μs after impact. The observed initial damage velocities are plotted against the projectile kinetic energy in Fig. 8. On the whole, the clear dependence of the damage velocities on impact energy is not observed under the same $t_t$ condition, although the internal failure velocities of 10-mm-thick glass only show a slight increase with the increase in projectile kinetic energy. The surface fracture velocities seem to be unaffected by the $t_t$ condition. The surface fracture is expected to be mainly caused by the rarefaction from the impact surface. Therefore, it is considered that the target thickness have an insignificant effect on the surface fracture velocity. In contrast the initial damage velocities of internal failure and conchoidal failure clearly show a decrease with the increase in $t_t$. In the case of the internal failure, the reverberation and interaction of rarefactions are expected to play important role. Such wave interactions occur more frequently in the thinner sample and it would result in acceleration the damage development.

The mean values of the measured damage velocities are listed together with the ratio of the damage velocities to the longitudinal and transversal sound velocities in Table 2. The sound velocities of $SiO_2$ glass are as follows: $C_l$ = 5.90 km/s, $C_t$ = 3.75 km/s. All damage velocities are slower than the transversal sound velocity. The damage velocity of surface fracture is about $0.3C_t$. In the case of internal failure, the damage velocity varies from $0.5C_t$ to $0.7C_t$ depending on target thickness. In the previous studies of edge-on-impact performed on some kinds of glasses [9-12], the damage velocities of

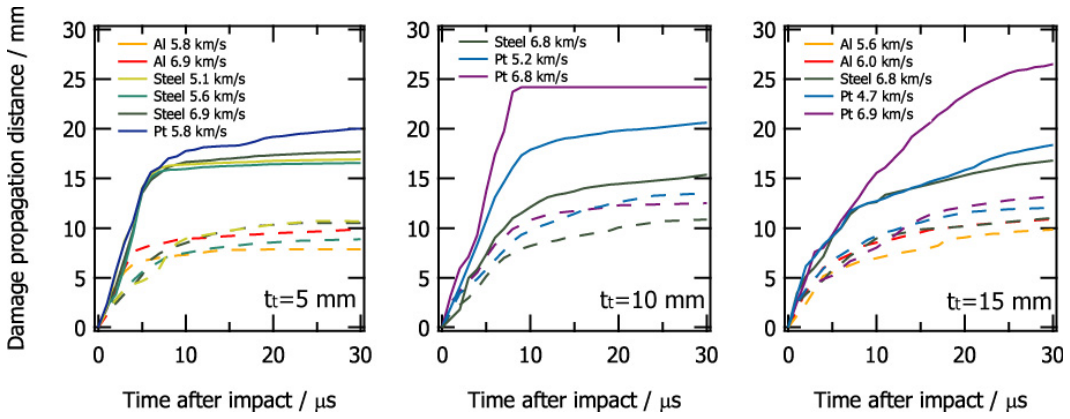


Fig. 7. Time evolution of damage propagation distance. The solid lines represent the internal failure. The dashed lines represent the surface fracture.

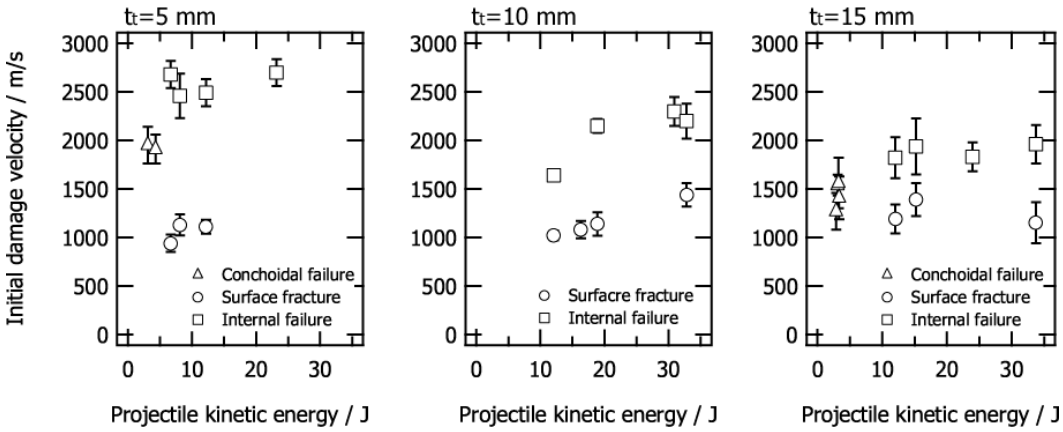


Fig. 8. The relationship between $KE_p$ and $v_D$.

Table 2. Mean values of the measured initial damage velocities for each $t_t$ with the ratios of the $v_D$ to $C_l$ and $C_t$.

| | $t_t$ / mm | $v_D$ / m/s | $v_D/C_l$ | $v_D/C_t$ |
|---|---|---|---|---|
| Surface fracture | 5 | 1060 | 0.18 | 0.28 |
| | 10 | 1170 | 0.20 | 0.31 |
| | 15 | 1240 | 0.21 | 0.33 |
| Internal failure | 5 | 2580 | 0.44 | 0.69 |
| | 10 | 2070 | 0.35 | 0.55 |
| | 15 | 1890 | 0.32 | 0.50 |

impact direction range from $C_t$ to $C_l$ and the damage velocities of vertical direction show the value close to $C_t$. The projectile used in these edge-on-impact tests is a steel-cylinder [9-11] or a tungsten-alloy-rod [12] which are several centimeters in size even though the target size is similar to that of this study. As a result, the input impact energy into the observation area of target is higher than that of this study although the impact velocities are considerably low, which range up to 1500 m/s. It is expected that the high input energy density causes the higher damage velocity than that of this study.

The propagation behavior of radial cracks are also analyzed from high-speed photograph and summarized in Fig. 9. In contrast to the internal and surface fracture, the propagation distance of radial crack show linear growth against time. Its propagation velocity which is derived by linear regression of the path-time data shows a correlation to $KE_p/t_t$. The results of this relation also show the threshold for radial crack formation, which is expected to be between 1.2 and 1.6 J/mm. The terminal crack velocity is theoretically predicted to be about $0.5C_t$ [13, 14]. The crack velocity observed in previous edge-on-impact studies show $0.45C_t$ as terminal velocity [9]. The radial crack velocity is also expected to approaches asymptotically to $0.45C_t$ with increasing $KE_p/t_t$.

## 4. Summary

Hypervelocity impact tests were conducted on a $SiO_2$ glass plate and the damage evolution was captured using a high-speed video camera. Appling a reflected light configuration, the propagation behavior of surface fracture and internal failure were simultaneously observed. The postmortem observation of the impacted target revealed the fracture patterns formed in the target, which were categorized into central pit, conchoidal failure, cone crack, internal failure, lateral crack, and radial crack. The time evolutions of surface fracture and internal failure showed initial rapid propagation followed by slow propagation. The propagation velocities of surface fracture showed nearly constant value regardless of impact conditions performed in this study. In contrast, the propagation velocities of internal failure decreased with increasing the target thickness. In the case of radial cracks, the cracks extended linearly with time. The radial crack velocity increased with increasing $KE_p/t_t$ and showed the tendency to approach asymptotically to $0.45C_t$ which is expected terminal velocity.

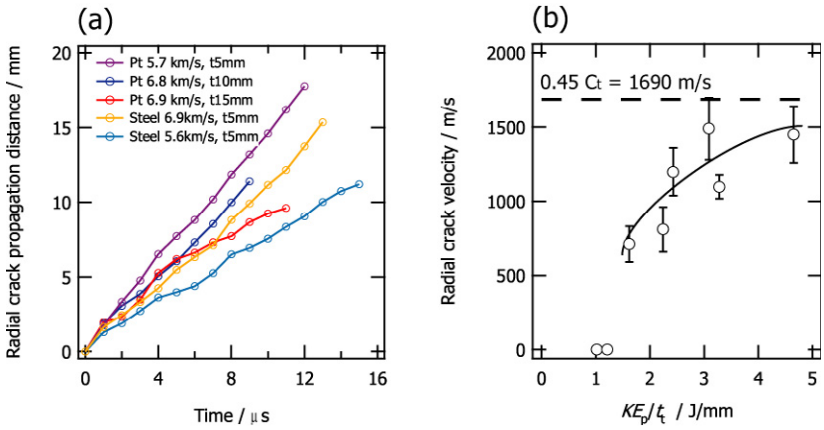


Fig. 9. The propagation behavior of radial cracks. (a) time evolution of propagation distance (b) the relationship between crack velocity and $KE_p/t_t$.

## Acknowledgements

This research was supported by the Space Plasma Laboratory, ISAS, JAXA.

## References

[1] Klinkrad, H., 2011, "Protecting the space debris environment and protecting against it," Proceedings of the 11th Hypervelocity Impact Symposium, pp. 171-181.
[2] Cour-Palais, E. G., 1999, A career in applied physics: apollo through space station, International Journal of Impact Engineering 23, p. 137.
[3] Christiansen, E. L., 1993, , International Journal of Impact Engineering 14, p. 145.
[4] Kawai, N., Tsurui, K., Shindo, D., Motoyashiki, Y., Sato, E., 2011, Fracture behavior of silicon nitride ceramics subjected to hypervelocity impact, International Journal of Impact Engineering 38, p. 542.
[5] Burt, R. R., Christiansen, E. L., 2003, Hypervelocity impact testing of transparent spacecraft materials, International Journal of Impact Engineering 29, p. 153.
[6] Schneider, E., Stilp, A. J., Kagerbauer, G., 1995, Meteoroid/debris simulation experiments on MIR viewport samples, International Journal of Impact Engineering 17, p. 731.
[7] Kawai, N., Tsurui, K., Hasegawa, S., Sato, E., 2010, Single microparticle launching method using two-stage light-gas gun for simulating hypervelocity impacts of micrometeoroids and space debris, Review of Scientific Instruments 81, 115105.
[8] Taylor, E. A., Tsembelis, K., Hayhurst, C. J., Kay, L., Burchell, M. J., 1999, Hydrocode modelling of hypervelocity impact on brittle materials: depth of penetration and conchoidal diameter, International Journal of Impact Engineering 23, p. 895.
[9] Strassburger, E., Senf, H.,1995, "Experimental investigations of wave and fracture phenomea in impacted ceramics and glasses," U. S. Army Research Laboratory contractor report ARL-CR-214.
[10] Strassburger, E., Patel, P., McCauley, J. W., Templeton, D. W., 2005, "High-speed photographic study of wave and fracture propagation in fused silica," Proceedings of the 22nd International Symposium on Ballistics, pp. 761-768.
[11] Strassburger, E., Patel, P., McCauley, J. W., Templeton, D. W., 2007, "Wave propagation and impact damage in transparent laminates," Proceedings of the 23rd International Symposium on Ballistics, pp. 1381-1388.
[12] Choi, J. H., Lee, C. H., Chang, S. N., Moon, S. K., 1995, Long-rod impact phenomena: role of wave interaction on crack propagation, International Journal of Impact Engineering 17, p. 195.
[13] Yoffe, E. H., 1951, The moving griffith crack, Philosophical Magazine 42, p. 739.
[14] Craggs, J. W., 1960, On the propagation of a crack in an elastic-brittle material, Journal of the Mechanics and Physics of Solids 8, p. 66.